Frontiers of Information Technology & Electronic Engineering
www.jzus.zju.edu.cn; engineering.cae.cn; www.springerlink.com
ISSN 2095-9184 (print); ISSN 2095-9230 (online)
E-mail: jzus@zju.edu.cn

Stepped frequency chirp signal imaging radar jamming using two-dimensional nonperiodic phase modulation*

Qihua WU†‡, Feng ZHAO†‡, Tiehua ZHAO, Xiaobin LIU, Junjie WANG, Shunping XIAO

State Key Laboratory of Complex Electromagnetic Environment Effects on Electronics and Information System, National University of Defense Technology, Changsha 410073, China

†E-mail: stevewoo1990@outlook.com; zhaofeng_nudt@163.com

Received July 11, 2022; Revision accepted Oct. 21, 2022; Crosschecked Feb. 23, 2023

Abstract: Stepped frequency chirp signal obtains high-resolution radar images by synthesizing multiple narrowband chirp pulses. It has been one of the most commonly used wideband radar waveforms due to its lower demand for radar instant bandwidth. In this paper, we propose a radar jamming method using two-dimensional nonperiodic phase modulation against stepped frequency chirp signal imaging radar. Using the unique property of nonperiodic phase modulation, the proposed method can generate high-level sidelobes that perform as a special blanket jamming along both the range and azimuth directions and make the target unrecognizable. Then, the influence of different modulation parameters, such as the code width and duty ratio, are further discussed. Based on this, the corresponding parameter design principles are presented. Finally, the validity of the proposed method is demonstrated by the Yake-42 plane data simulation and measured unmanned aerial vehicle data experiment.

Key words: Radar jamming; Stepped frequency chirp signal; Nonperiodic phase modulation; Wideband radar
https://doi.org/10.1631/FITEE.2200298 **CLC number:** TN95

1 Introduction

Wideband radar, such as synthetic aperture radar (SAR) and inverse SAR (ISAR), plays a significant role in both civil and military aspects due to its all-weather, all-day imaging ability over a long distance (Moradikia et al., 2019; Rong et al., 2019; Kang et al., 2021). To avoid the target being detected and observed by wideband radar, jamming methods against wideband radar have been developed rapidly in recent decades.

Wideband radar jamming changes mainly the radar imaging feature by modulating the intercepted radar signal in the time, frequency, and phase domain. Generally, the jamming method can be divided into two different effects, blanket jamming and deception jamming. Blanket jamming covers mainly the whole radar image or some critical parts with wideband noise and makes the target unrecognizable (Tai et al., 2016). Deception jamming confuses mainly the victim radar by generating some misguided information such as multifalse targets (Pan et al., 2014; Wang W et al., 2014; Bo et al., 2015). Recently, some novel jamming methods, such as active echo cancellation (Meller, 2012; Xu LT et al., 2015; Wu et al., 2018) and passive electromagnetic metamaterial modulation (Wang JJ et al., 2021, 2022), have also attracted great attention.

The wideband chirp (linear frequency modulation, LFM) signal is the most commonly used imaging radar waveform due to its large time-bandwidth product (TBP). Hence, most wideband radar jamming methods have been proposed for chirp signals, such as

‡ Corresponding authors
* Project supported by the Natural Science Foundation of Hunan Province, China (No. 2022JJ40561), the Scientific Research Program of National University of Defense Technology, China (No. ZK22-46), and the National Natural Science Foundation of China (Nos. 61890542, 62001481, and 62071475)
ORCID: Qihua WU, https://orcid.org/0000-0002-9998-2301; Feng ZHAO, https://orcid.org/0000-0003-1275-3352

frequency shifting jamming (Huang and Chan, 2021; Zhao et al., 2021) and interrupted-sampling repeater jamming (ISRJ) (Wang XS et al., 2007; Feng et al., 2011, 2017). In recent decades, with the proposal and development of synthetic wideband theory, many kinds of synthetic wideband waveforms have been applied to wideband radar. Stepped frequency chirp signals achieve high-resolution imaging by synthesizing a train of narrowband chirp pulses (Zhang L et al., 2011; Zhou et al., 2021; Wang C et al., 2022; Wang Y et al., 2022). Since the stepped frequency chirp signal reduces the demand for radar instant transmitting bandwidth, it has been widely applied in wideband radar imaging. Hence, it is of vital significance to explore target protection methods against stepped frequency chirp signal radar.

In our previous work, the radar jamming method using the nonperiodic ISRJ technique was proposed against wideband chirp radars (Wu et al., 2019). It can generate high-level sidelobes that perform blanket jamming after imaging processing by nonperiodic ISRJ modulation instead of multifalse-target deception with conventional uniform ISRJ. However, the ISRJ technique is essentially the "0–1" modulation in the amplitude domain, which inevitably brings energy loss (Wang XS et al., 2007). Inspired by our previous work, a jamming method against stepped frequency chirp signal radar using nonperiodic phase modulation is proposed in this paper. On one hand, the proposed "±1" modulation in the phase domain instead of the "0–1" modulation in the amplitude domain avoids energy loss and makes a more efficient use of the jamming power. On the other hand, the modulation method on the stepped frequency chirp signal is further expanded according to its subpulse synthetic property compared with the chirp signal. By nonperiodic phase modulation on a stepped frequency chirp signal in both fast and slow time domains, a flexible two-dimensional (2D) blanket jamming performance is obtained.

2 Imaging model of stepped frequency chirp signals

As shown in Fig. 1, the stepped frequency chirp signal contains N narrowband chirp subpulses with frequency stepping. The frequency of the i^{th} subpulse can be given by $f_i=f_0+i\Delta f$, where $i=0, 1, \cdots, N-1$, f_0 is the carrier frequency, and Δf is the frequency interval between the adjacent subpulses. Then, the stepped frequency chirp signal can be written as

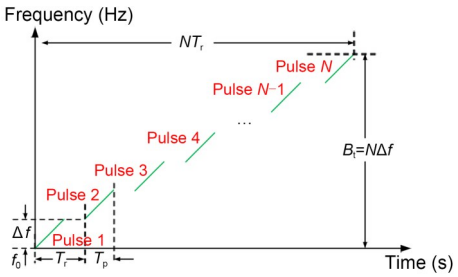

Fig. 1 Stepped frequency chirp radar signal

$$s(t)=\sum_{i=0}^{N-1}\left(\operatorname{rect}\left(\frac{t-iT_{\mathrm{r}}}{T_{\mathrm{p}}}\right)\cdot\exp\left(\mathrm{j}2\pi f_i(t-iT_{\mathrm{r}})+\mathrm{j}\pi k_{\mathrm{r}}(t-iT_{\mathrm{r}})^2\right)\right), \tag{1}$$

where t is the fast time variable, T_{r} represents the subpulse repetition interval, T_{p} is the subpulse width, $k_{\mathrm{r}}=B/T_{\mathrm{p}}$ is the chirp rate, and B is the subpulse bandwidth.

Assuming that the distance between the radar and the target is R, then the target echo can be given by

$$\begin{aligned}s_{\mathrm{r}}(t)&=\sigma s(t-\tau_{\mathrm{d}})\\&=\sigma\sum_{i=0}^{N-1}\operatorname{rect}\left(\frac{t_i}{T_{\mathrm{p}}}\right)\exp\left(\mathrm{j}2\pi f_i t_i+\mathrm{j}\pi k_{\mathrm{r}}t_i^2\right),\end{aligned} \tag{2}$$

where $t_i=t-\tau_{\mathrm{d}}-iT_{\mathrm{r}}$, $\tau_{\mathrm{d}}=2R/c$ denotes the time delay, σ is the target radar cross-section (RCS), and c is the propagation velocity of the electromagnetic wave.

After the radar receives the target echo, pulse compression (PC) processing is executed for each subpulse. According to the property of the chirp signal, the PC output of the i^{th} subfrequency can be given by

$$y(t,i)=\sigma\sqrt{BT_{\mathrm{p}}}\operatorname{sinc}\left(\pi B(t-iT_{\mathrm{r}}-\tau_{\mathrm{d}})\right)\exp(-\mathrm{j}2\pi f_i\tau_{\mathrm{d}}). \tag{3}$$

The sampling moment is $t=iT_{\mathrm{r}}+\tau_{\mathrm{d}}$. Then, the sampler of $y(t, i)$ is

$$\begin{aligned}e(i)&=\sigma\sqrt{BT_{\mathrm{p}}}\exp(-\mathrm{j}2\pi f_i\tau_{\mathrm{d}})\\&=\sigma\sqrt{BT_{\mathrm{p}}}\exp(-\mathrm{j}2\pi(f_0+i\Delta f)\tau_{\mathrm{d}}).\end{aligned} \tag{4}$$

By conducting the N-point discrete Fourier transform (DFT) to $e(i)$, the high-resolution range profile (HRRP) can be given by

$$h(k)=\sigma\sqrt{BT_{\mathrm{p}}}\exp(-\mathrm{j}2\pi f_0\tau_{\mathrm{d}})\mathrm{sinc}\big(\pi(k-N\Delta f\tau_{\mathrm{d}})\big). \quad (5)$$

The peak value of Eq. (5) can be obtained at $k_0=N\Delta f\tau_{\mathrm{d}}$, and the range resolution is $\rho_{\mathrm{r}}=\dfrac{c}{2N\Delta f}$. The equivalent bandwidth is $B_{\mathrm{t}}=N\Delta f$. The unambiguous imaging range can be given by

$$R_{\mathrm{ua}}\in\left[-\frac{c}{4\Delta f},\frac{c}{4\Delta f}\right]. \quad (6)$$

Then, the maximum imaging size of the stepped frequency chirp signal in the range direction is

$$\Delta R_{\mathrm{r}}=\frac{c}{2\Delta f}. \quad (7)$$

After the HRRP $h(k)$ is obtained, the 2D target image can be further acquired by azimuth imaging processing.

Assume that there are M observations for azimuth imaging. The m^{th} observation can be written as $h(k, t_m)$, where $t_m=mT_{\mathrm{d}}$ is the slow time variable, T_{d} is the dwell time within one aperture, and m is an integer that satisfies $1\le m\le M$. Then $h(k, t_m)$ can be given by (Zhang Q et al., 2008)

$$h(k,t_m)=\sigma\sqrt{BT_{\mathrm{p}}}\exp(-\mathrm{j}2\pi f_0\tau_{\mathrm{d}})\cdot\mathrm{sinc}\big(\pi(k-N\Delta f\tau_{\mathrm{d}})\big)\exp\left(\frac{-\mathrm{j}4\pi\omega p_y}{\lambda}t_m\right), \quad (8)$$

where p_y is the ordinate of the target in the azimuth direction, λ is the radar wavelength, and ω is the target rotation angular velocity.

After range alignment and phase adjustment processing (Xu G et al., 2015), the 2D image $I(k, m)$ can be obtained by the M-point fast Fourier transform (FFT) operation in slow time domain (Zhang Q et al., 2008; Luo et al., 2010):

$$I(k,m)=\mathrm{FFT}(h(k,t_m),m)=\sigma\sqrt{BT_{\mathrm{p}}}\exp(-\mathrm{j}2\pi f_0\tau_{\mathrm{d}})\cdot\mathrm{sinc}\big(\pi(k-N\Delta f\tau_{\mathrm{d}})\big)\mathrm{sinc}\left(2\pi\left(m-\frac{2\omega T_{\mathrm{A}}p_y}{\lambda}\right)\right), \quad (9)$$

where $T_{\mathrm{A}}=MT_{\mathrm{d}}$ is the imaging observation time.

The peak value of Eq. (9) in the azimuth direction is obtained at $m_0=\dfrac{2\omega T_{\mathrm{d}}p_y}{\lambda}$. The azimuth resolution is $\rho_{\mathrm{a}}=\dfrac{\lambda}{2\omega MT_{\mathrm{d}}}$. Then the maximum imaging area of the stepped frequency chirp signal in the azimuth direction is

$$\Delta R_{\mathrm{a}}=M\rho_{\mathrm{a}}=\frac{\lambda}{2\omega T_{\mathrm{d}}}. \quad (10)$$

According to the imaging procedure given above, the processing procedure of the wideband chirp signal and the stepped frequency chirp signal differs mainly in the HRRP acquisition in the fast time domain, which can be concluded in Fig. 2.

As shown in Fig. 2, the conventional wideband chirp signal can obtain the HRRP directly after PC processing. The stepped frequency chirp signal requires two-stage processing. Stage 1 is to obtain the coarse resolution range profiles (CRRPs) by PC operation on the subpulses. Stage 2 is to finally acquire the HRRP by the multipulse synthesis of the CRRPs.

Frankly, the processing procedure of the chirp signal is comparatively simple. However, as stated in Section 1, the main innovation of the stepped frequency chirp signal is to reduce the instant bandwidth demand on the radar system. For instance, to achieve a 500 MHz imaging bandwidth, if the chirp signal is used, the bandwidth of the chirp pulse should be 500 MHz, and then the instant bandwidth demand on the radar transmitter will be at least 500 MHz. However, when the stepped frequency chirp signal is used, by transmitting 100 subpulses with 5 MHz frequency interval, the bandwidth of a single subpulse could be even smaller than 5 MHz. Then, the instant bandwidth demand on the radar transmitter can also be smaller than 5 MHz. It greatly reduces the hardware cost for wideband imaging by applying the stepped frequency chirp signal. In addition, it also makes the narrowband radar achieve wideband imaging ability, which is of great value in some practical applications.

Note that the unique two-stage processing procedure of the stepped frequency chirp signal has a different jamming requirement. The corresponding analyses are given in Section 3.

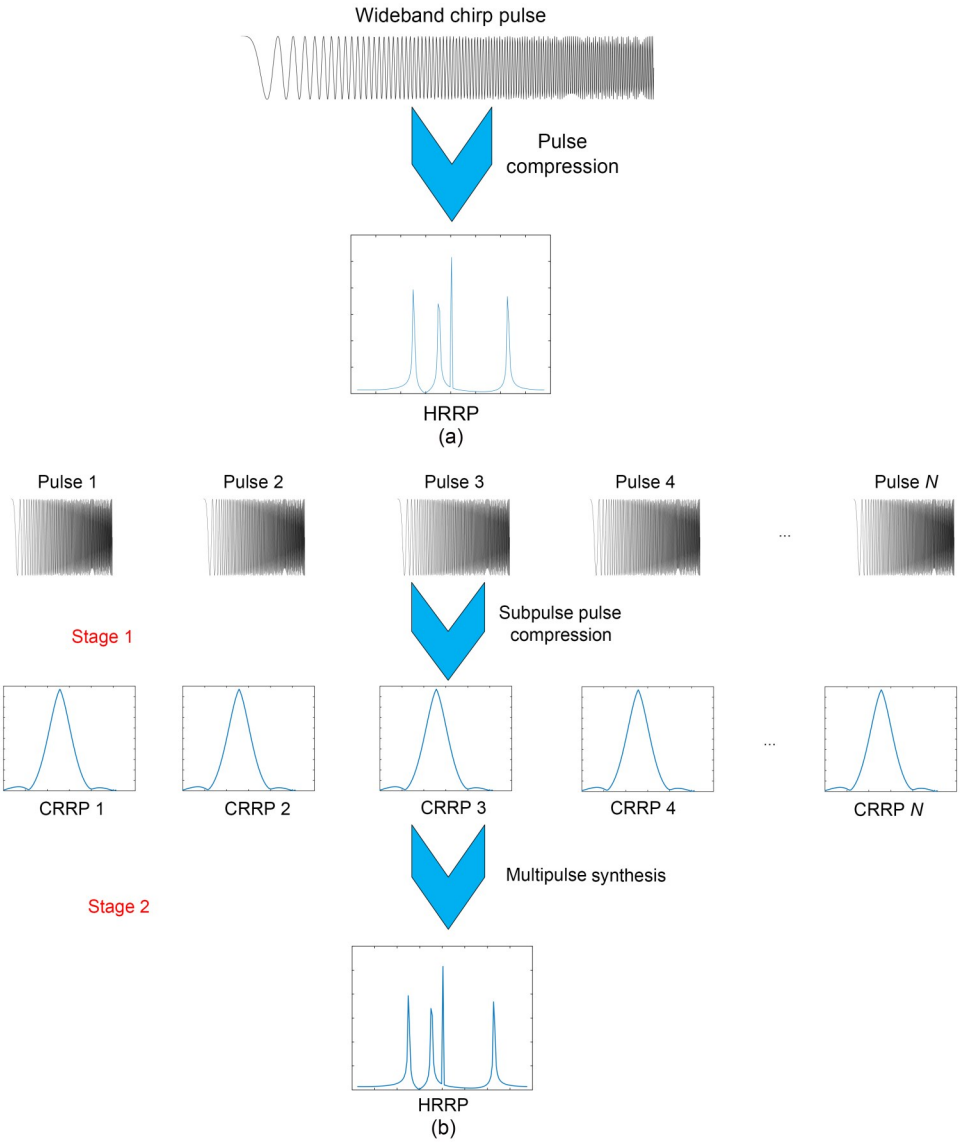

Fig. 2 Imaging procedure difference between the wideband chirp signal (a) and the stepped frequency chirp signal (b) (CRRP: coarse resolution range profile; HRRP: high-resolution range profile)

3 The proposed jamming method

3.1 Property of nonperiodic phase modulation

As shown in Fig. 3, the nonperiodic phase modulation is a rectangular pulse train encoded by {+1, −1}, given by

$$p(t)=\mathrm{rect}\left(\frac{t}{\tau}\right)\otimes\sum_{n=-\infty}^{+\infty}a_n\delta(t-n\tau), \tag{11}$$

where τ is the code width, "⊗" is the convolution operation, $\delta(\cdot)$ is the ideal impulse function, and a_n is the phase sequence encoded by {+1, −1} (here, +1 codes denote the positive phase modulation, and −1 codes denote the opposite phase modulation). According to the above assumptions, the code number within one pulse can be expressed as $N_R=T/\tau$, where T is the pulse width of the modulated signal. In addition, the duty ratio η is defined as the proportion of +1 codes.

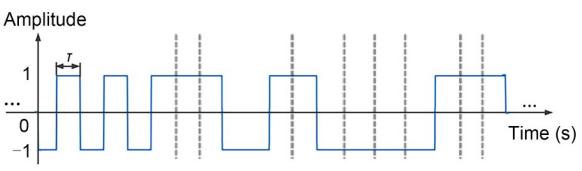

Fig. 3 Nonperiodic phase modulation pulse

By applying the FFT to Eq. (11), the frequency spectrum is

$$P(f)=\tau\,\mathrm{sinc}(\tau f)\sum_{n=0}^{N_R-1}a_n\exp(-\mathrm{j}2\pi n\tau f). \quad (12)$$

When f=0, the peak output of the frequency spectrum is

$$P(0)=N_R\tau|1-2\eta|. \quad (13)$$

From Eq. (13), the peak output is related only to the duty ratio. Specifically, when η=0.5, the peak output will disappear.

In addition, the nonperiodic phase modulation brings continuous frequency removal. When $f=nf_s$, $P(f)$=0, where n is a nonzero integer and f_s is the phase modulation frequency. The main-lobe bandwidth is

$$B_{\mathrm{main}}=2/\tau. \quad (14)$$

The above analyses indicate that when the radar signal is modulated by the nonperiodic phase pulse, it is equivalent to shifting the radar signal in the continuous frequency domain. Specifically, for the wideband chirp signal, the high-level sidelobes will spread along the range direction after PC processing due to its time-delay Doppler coupling property. It can be used as a special blanket jamming in the radar image.

3.2 Jamming method using nonperiodic phase modulation against stepped frequency chirp radar

3.2.1 Nonperiodic phase modulation in the fast time domain

As analyzed in Section 2, different from the conventional wideband chirp signal, the stepped frequency chirp signal achieves wideband imaging by synthesizing a series of narrowband subpulses via a two-stage processing procedure. If the nonperiodic phase modulation is executed within every single subpulse, jamming is performed at stage 1. Then, the energy will spread along the CRRPs, which means that little energy successfully enters the range bin where the target is located after multipulse synthetic processing at stage 2. As a result, high-level blanket jamming will not be formed in the range direction. However, if the nonperiodic phase modulation is executed among the whole pulse trains, jamming is performed directly at stage 2. The jamming energy can all effectively enter the HRRP. Then, high-level blanket jamming can be formed.

Based on the above analyses, the jamming method using subpulse nonperiodic phase modulation in the fast time domain is proposed, as shown in Fig. 4.

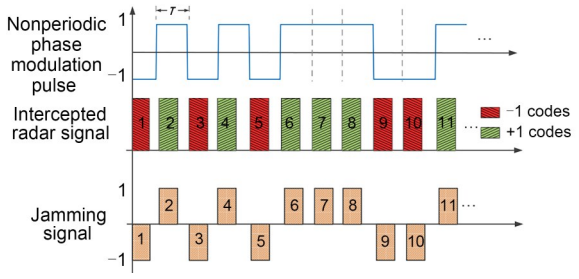

Fig. 4 Subpulse nonperiodic phase modulation in the fast time domain

As shown in Fig. 4, when the nonperiodic phase modulation is executed at the level of subpulses, the modulation code width should be integer multiples of T_r; i.e., $\tau=N_1T_r$, where N_1 is a nonzero integer.

According to the above assumptions, the stepped frequency chirp radar signal after nonperiodic phase modulation can be given by

$$s_j(t)=p(t)s(t). \quad (15)$$

Then, the CRRP after subpulse PC processing given in Eq. (4) is

$$m_j(i)=p(i)m(i), \quad (16)$$

where $p(i)$ is the discrete sampling of $p(t)$ for the i^{th} subpulse, and it can be written as

$$p(i)=\mathrm{rect}\left(\frac{i}{N_1}\right)\otimes\sum_{k=-\infty}^{+\infty}a_k\delta(i-nN_1). \quad (17)$$

According to the Fourier transform relationship in Eq. (12), the N-point DFT of Eq. (17) can be given by

$$P(k)=\frac{N_1}{N}\mathrm{sinc}\left(\frac{N_1}{N}k\right)\sum_{n=0}^{N_R-1}a_n\exp\left(-\mathrm{j}2\pi n\frac{N_1}{N}k\right). \quad (18)$$

Specifically, when k=0, we have

$$P(0)=\left|1-2\eta\right|. \tag{19}$$

Then, the HRRP of the jamming signal can be obtained by the N-point DFT to Eq. (16); that is

$$\begin{aligned} h_{\mathrm{j}}(k)&=\mathrm{DFT}(m_{\mathrm{j}}(i))=\mathrm{DFT}(m(i))\otimes\mathrm{DFT}(p(i))\\ &=h(k)\otimes P(k)=\frac{N_1}{N}h(k)\\ &\otimes\left(\sin\mathrm{c}\left(\frac{N_1}{N}k\right)\sum_{n=0}^{N_{\mathrm{R}}-1}a_n\exp\left(-\mathrm{j}2\pi n\frac{N_1}{N}k\right)\right). \end{aligned} \tag{20}$$

According to the properties of the convolution computation, Eq. (20) can be rewritten as

$$\begin{aligned} h_{\mathrm{j}}(k)&=P(0)h(k)+\sum_{i=-\infty,i\neq k}^{i=+\infty}h(i)P(k-i)\\ &=h_1(k)+h_2(k). \end{aligned} \tag{21}$$

As shown in Eq. (21), the HRRP of the jamming signal can be divided into two parts. The former part is

$$h_1(k)=P(0)h(k)=\left|1-2\eta\right|h(k), \tag{22}$$

which indicates that the signal HRRP after nonperiodic phase modulation will still has a peak output with the coefficient given by

$$\alpha=\left|1-2\eta\right|. \tag{23}$$

The latter part is

$$h_2(k)=\sum_{i=-\infty,i\neq k}^{i=+\infty}h(i)P(k-i). \tag{24}$$

According to the property of nonperiodic phase modulation given in Section 3.1, Eq. (24) corresponds to the part of continuous frequency modulation, which will generate high-level blanket sidelobes along the range direction in the radar image. From Eq. (20), the positions of zero points are

$$k_p=\frac{N}{N_1}p, \tag{25}$$

where p is an integer.

Then, the main blanket coverage can be given by

$$k_{\mathrm{main}}=k_{+1}-k_{-1}=\frac{2N}{N_1}. \tag{26}$$

3.2.2 Nonperiodic phase modulation in the slow time domain

From the above analyses, the nonperiodic phase modulation on the subpulses of the stepped frequency chirp signal in the fast time domain will generate a continuous blanket jamming strip. However, the line-shaped blanket strip along the range direction cannot supply effective azimuth protection in the 2D radar image. Hence, the nonperiodic phase modulation in the slow time domain is further conducted.

Similar to the modulation in the fast time domain in Eq. (17), the nonperiodic phase modulation pulse can be given by

$$q(t_m)=\mathrm{rect}\left(\frac{t_m}{\tau_{\mathrm{A}}}\right)\otimes\sum_{l=0}^{N_{\mathrm{A}}-1}b_l\delta(t_m-l\tau_{\mathrm{A}}), \tag{27}$$

where $N_{\mathrm{A}}=T_{\mathrm{A}}/\tau_{\mathrm{A}}$ denotes the code number in the slow time domain, and τ_{A} is the code width in the slow time domain. Similarly, τ_{A} should be integer multiples of the dwell time T_{d} to guarantee effective coding. b_l is the slow time code sequence. Then, the slow time duty ratio η_{A} can be defined as the proportion of +1 codes in b_l.

Considering the slow time domain, the jamming signal after fast time domain modulation in Eq. (15) can be rewritten as $s_{\mathrm{j}}(t, t_m)$. Then the signal after slow time domain modulation can be given by

$$s_{\mathrm{j1}}(t,t_m)=q(t_m)s_{\mathrm{j}}(t,t_m). \tag{28}$$

The azimuth HRRP can be obtained by FFT to Eq. (28). Similar to the fast time domain, the blanket jamming strip will spread along the azimuth direction due to the slow time nonperiodic phase modulation.

The peak output after slow time modulation has the coefficient of

$$\alpha_{\mathrm{A}}=\left|1-2\eta_{\mathrm{A}}\right|. \tag{29}$$

The coverage in the azimuth direction can be given by

$$m_{\mathrm{main}}=\frac{2M}{M_1}, \tag{30}$$

where $M_1=\tau_A/T_d$ denotes the aperture number within one slow time modulation pulse.

3.2.3 The proposed jamming procedure

As analyzed above, after nonperiodic phase modulation in both fast and slow time domains, the 2D blanket area will spread along the range and azimuth directions for stepped frequency chirp signal radar. The typical scene is shown in Fig. 5.

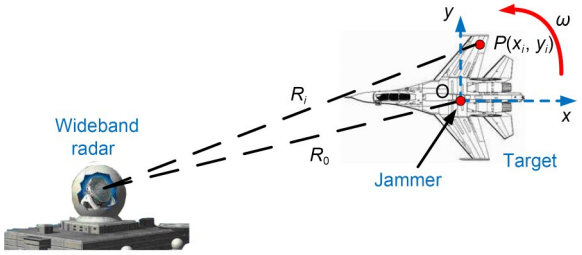

Fig. 5 Geometric relationship of the radar, target, and jammer

As shown in Fig. 5, the jammer is fixed on the center of the target, which intercepts and modulates the radar signal and protects the target by transforming the target image feature. The whole procedure can be concluded in Fig. 6.

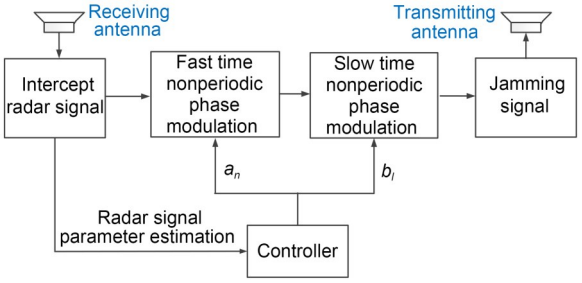

Fig. 6 The proposed jamming procedure

First, the jammer intercepts the radar signal by the receiving antenna. Then, the controller analyzes the signal parameter and modulates the radar signal in both fast and slow time domains with the phase codes a_n and b_l, respectively. Finally, the jamming signal is retransmitted back to the victim radar after power amplification.

3.3 Jamming feature analyses

3.3.1 Coverage of the blanket area

According to the analyses given in Eqs. (26) and (30), the coverage of the blanket strips in the 2D radar image can be given by

$$\Delta r=\frac{c}{2B_t}k_{\text{main}}=\frac{c}{N_1\Delta f}=\frac{cT_r}{\Delta f\tau}, \tag{31}$$

$$\Delta a=\frac{\lambda}{2\omega T_A}m_{\text{main}}=\frac{\lambda}{\omega\tau_A}, \tag{32}$$

where Δr and Δa are the coverages in the range and azimuth directions, respectively.

Then, the whole size can be given by

$$\Delta S=\Delta r\Delta a=\frac{cT_r\lambda}{\omega\Delta f\tau\tau_A}. \tag{33}$$

According to Eqs. (31)–(33), the coverage of the jamming strips is determined mainly by two series of parameters. One is the stepped frequency chirp signal parameter, and the other is the phase modulation parameter. For the former factor, the ratio of the frequency interval Δf to the subpulse repetition interval T_r determines the coverage in the range direction, which can also be defined as the equivalent chirp rate $k'=\Delta f/T_r$. A larger wavelength λ is beneficial to obtain a larger coverage in the azimuth direction. For the latter factor, the smaller the phase modulation code widths τ and τ_A, the larger the jamming coverage.

3.3.2 Average blanket jamming power

Assume that the peak power of the jammer is P_j and the antenna gain is G_j. Then the energy density of the jamming signal arriving at the radar is

$$S_j=\frac{P_jG_j}{4\pi R_0^2}, \tag{34}$$

where R_0 is the distance between the radar and jammer.

After radar imaging processing, the total jamming power during the whole observation can be given by

$$P_{rj}=MS_jG_r\lambda^2G_{pc}=\frac{MP_jG_jG_r\lambda^2G_{pc}}{4\pi R_0^2}, \tag{35}$$

where $G_{pc}=NB_tT_r$ is the PC gain of the stepped frequency chirp signal and G_r is the radar receiving antenna gain.

The jamming power given in Eq. (35) can be approximatively assumed to be located mainly in the area given by Eq. (33). Hence, the average blanket power in the image is

$$P_{ave}=\frac{P_{rj}}{\Delta S}==\frac{MP_jG_jG_r\lambda B_t^2\omega\tau\tau_A}{4\pi cR_0^2}. \tag{36}$$

From Eq. (36), it is obvious that the larger code widths τ and τ_A are more beneficial to obtain a larger average blanket jamming power. This is because larger code widths τ and τ_A mean smaller coverage of the blanket area. Then, the energy can receive a better focus.

3.4 Jamming parameter setting principles

3.4.1 Selection of the code widths

According to Eq. (36), the larger modulation code widths τ and τ_A are beneficial factors for the proposed jamming method. However, the generated blanket area should cover the whole target in the radar image to make it unrecognizable. Assume that the lengths of the target in the range and azimuth directions are L_R and L_A, respectively. Then

$$\Delta r\geq L_R, \tag{37}$$

$$\Delta a\geq L_A. \tag{38}$$

Then, the code widths should satisfy

$$\tau\leq\frac{cT_r}{L_R\Delta f}, \tag{39}$$

$$\tau_A\leq\frac{\lambda}{L_A\omega}. \tag{40}$$

On the other hand, due to the unique property of the stepped frequency chirp signal, to make the blanket jamming performance better, the coverage in the range direction should be within the unambiguous imaging range given by Eq. (7). Then, we have

$$\Delta r\leq\Delta R_r. \tag{41}$$

Then, the code width should satisfy

$$\tau\geq 2T_r, \tag{42}$$

indicating that the code width should be at least twice as large as the subpulse repetition interval, which also demonstrates that the phase modulation should be among the whole pulse trains, not within the single subpulse.

Similarly, the coverage in the azimuth direction should be within the range given by Eq. (10). Then, we have

$$\Delta a\leq\Delta R_a. \tag{43}$$

Then, the code width in the slow time domain should satisfy

$$\tau_A\geq 2T_d. \tag{44}$$

In addition, as analyzed in Section 3.2, the fast and slow time code widths must be integer multiples of the subpulse repetition interval T_r and the dwell time T_d, respectively. Hence, the code widths τ and τ_A should be selected under this condition within the limits given by Eqs. (39), (40), (42), and (44).

3.4.2 Selection of the duty ratios

As analyzed in Section 3.2, the signal after nonperiodic phase modulation will still have a peak output with the coefficient given by Eqs. (23) and (29). It will form a bright line after radar imaging processing, which seriously affects the jamming performance. To avoid this, the duty ratio should be specially selected to make the peak output disappear. Then, we have

$$\alpha=\left|1-2\eta\right|=0, \tag{45}$$

$$\alpha_A=\left|1-2\eta_A\right|=0. \tag{46}$$

Then, the duty ratios should satisfy

$$\eta=0.5, \tag{47}$$

$$\eta_A=0.5. \tag{48}$$

Eqs. (47) and (48) indicate that the peak output of nonperiodic phase modulation will disappear when η=0.5 and η_A=0.5 due to the precise cancellation of +1 codes and −1 codes, respectively.

3.5 Jamming flow chart

According to the above analyses, the proposed jamming flow chart can be concluded in Fig. 7.

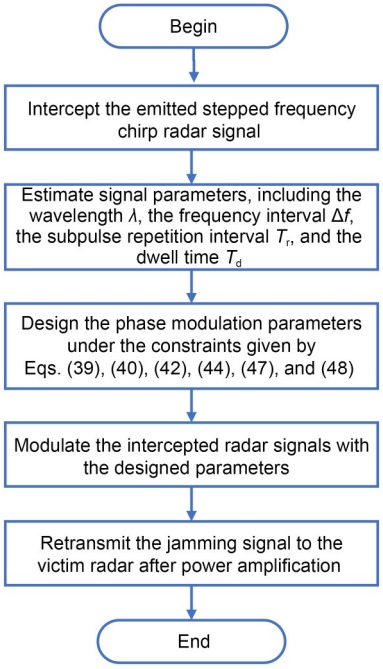

Fig. 7 The proposed jamming flow chart

4 Simulation results

In this section, the proposed jamming method is verified by 330-point Yake-42 plane data simulations, as shown in Fig. 8a. The distance between the radar and the plane is R_0=100 km, the radar peak power is P_t=1 mW, the transmit and receive antenna gains are G_t=G_r=30 dB, the target RCS is σ=10 m^2, and the rotation angular velocity is ω=0.05π rad/s. The transmitted radar stepped frequency chirp signal has a radio frequency f_0=10 GHz, the subpulse width is T_p=1 μs, the bandwidth is B=1 MHz, and the chirp rate is k_r=B/T_p=10^{12} Hz/s. The subpulse repetition interval is T_r=5 μs, the total subpulse number is N=128, the frequency interval of adjacent subpulses is Δf=2 MHz, and the equivalent bandwidth is B_t=$N\Delta f$=256 MHz. The aperture number for azimuth imaging is M=256, and the dwell time within one aperture is T_d=1 ms.

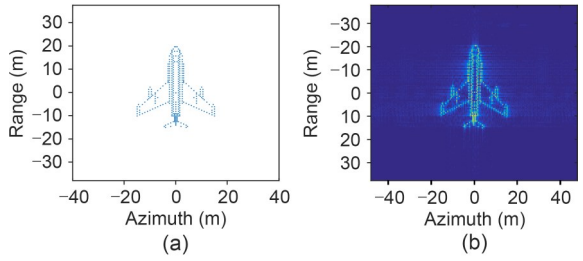

Fig. 8 The Yake-42 plane model: (a) target model; (b) original imaging result

The original imaging result is shown in Fig. 8b. The lengths of the target in the range and azimuth directions are L_R=35 m and L_A=30 m, respectively. The plane is clearly visible in the image before being jammed.

To conduct the nonperiodic phase modulation jamming method, put the jammer on the center of the plane, i.e., (0, 2.5) m in the image. Assume that the transmitting antenna gain is G_j=20 dB.

4.1 Jamming performances with different code widths

First, the jamming performances with different code widths are presented in this subsection. Assume that the transmitting power of the jammer is P_j=20 W. Fig. 9 presents the jammed image with different code widths.

As shown in Fig. 9, the jammed radar image is covered by square-shaped blanket strips spreading along both the range and azimuth directions. The plane becomes less visible and recognizable compared with the original imaging result in Fig. 8b. Hence, the effectiveness of the proposed jamming method is demonstrated.

In addition, it is obvious that smaller code widths result in larger blanket coverage, which is consistent with the theoretical analysis. The generated blanket sidelobes can completely cover the target and make it unrecognizable when code widths are set as τ=10 μs, τ_A=2 ms and τ=20 μs, τ_A=4 ms as shown in Figs. 9a and 9b, respectively. As shown in Fig. 9b, due to the smaller blanket coverage, the target is better protected and is less visible because of the larger average blanket power compared with the performance in Fig. 9a. However, when the code width increases, although a larger average power can be obtained, the plane is still visible in the image because the target is not completely covered, as shown in Fig. 9c. According to Eqs. (39) and (40), the code widths should satisfy $\tau \le 25$ μs and $\tau_A \le 6.3$ ms to cover the whole target, which is consistent with the results presented in Fig. 9. According to the simulations, to obtain the best jamming performance, the code

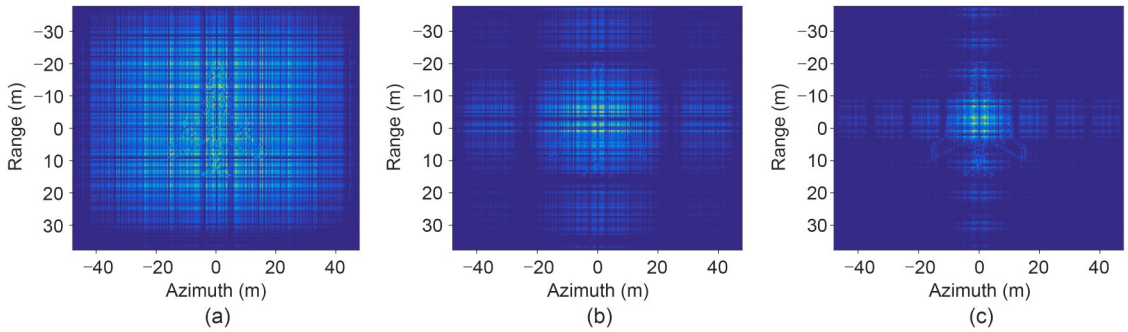

Fig. 9 Jamming performances with different code widths: (a) τ=10 μs, τ_A=2 ms; (b) τ=20 μs, τ_A=4 ms; (c) τ=40 μs, τ_A=8 ms

width should be selected to exactly cover the target and can also guarantee the largest average power in practice.

4.2 Jamming performances with different powers

Fig. 10 presents the jamming performances with different jamming powers. Assume τ=20 μs and τ_A=4 ms for the proposed method. For comparison, the jamming performances of the ISRJ-based method (Wu et al., 2019) and conventional noise jamming with the same power are presented, where the parameters of the ISRJ-based method are the same as those of the proposed method, and the noise jamming bandwidth is assumed to be the same as the radar signal bandwidth, B_j=B_t=256 MHz.

As shown in Fig. 10, the blanket jamming performance worsens with decreasing jamming power for all methods, which is consistent with our common sense. However, the proposed method in this study is obviously better than both the ISRJ-based method and the conventional noise jamming method. When the transmitting power reaches P_j=50 W, the plane can be clearly distinguished in the image for the conventional noise jamming method, while for the ISRJ-based method, even though the plane is mostly shielded, but still slightly visible, as shown in Fig. 10b. For comparison, when the transmitting power of our proposed method is P_j=50 W, the plane is perfectly shielded. Even when the transmitting power decreases to P_j=5 W, only the outline of the plane is slightly visible in the image and is obviously unrecognizable, while it can be clearly distinguished for both the other two methods, as shown in Fig. 10c. There are two main reasons contributing to the superior performance of our proposed method compared with noise jamming. On one hand, the jamming signal of our proposed method is coherent to the radar signal; then the coherent processing gain can be obtained, while the noise jamming method cannot gain this advantage. On the other hand, the jamming energy of our proposed method can be focused on a relatively small area by code width designs; then, a larger average power can be obtained, while the power of the noise jamming method is distributed in the whole imaging area. In addition, when compared with the ISRJ-based method, the proposed method also obtains an obviously higher blanket level. This is because the proposed method obtains more efficient use of the jamming power by the "±1" modulation in the phase domain, while the ISRJ-based method uses mainly the "0–1" modulation in the amplitude domain, which causes energy loss due to the transmitting of only parts of the whole pulses.

4.3 Performance evaluation

In this subsection, the jamming performance of the proposed method is quantitatively evaluated using the average suppression ratio, which can be defined as follows:

$$r_{sj}=10\lg\frac{\sum_{i=m_1}^{m_2}\sum_{j=n_1}^{n_2}I^2(i,j)-\sum_{i=m_1}^{m_2}\sum_{j=n_1}^{n_2}I_0^2(i,j)}{\sum_{i=m_1}^{m_2}\sum_{j=n_1}^{n_2}I_0^2(i,j)}, \quad (49)$$

where m_1 and m_2 are the starting point and ending point along the range direction in the image respectively, and n_1 and n_2 are the starting point and ending point along the azimuth direction in the image respectively. $I(i, j)$ is the pixel value of the jammed image, while $I_0(i, j)$ is the pixel value of the original unjammed image. By definition, the larger the average suppression ratio, the better the suppression performance.

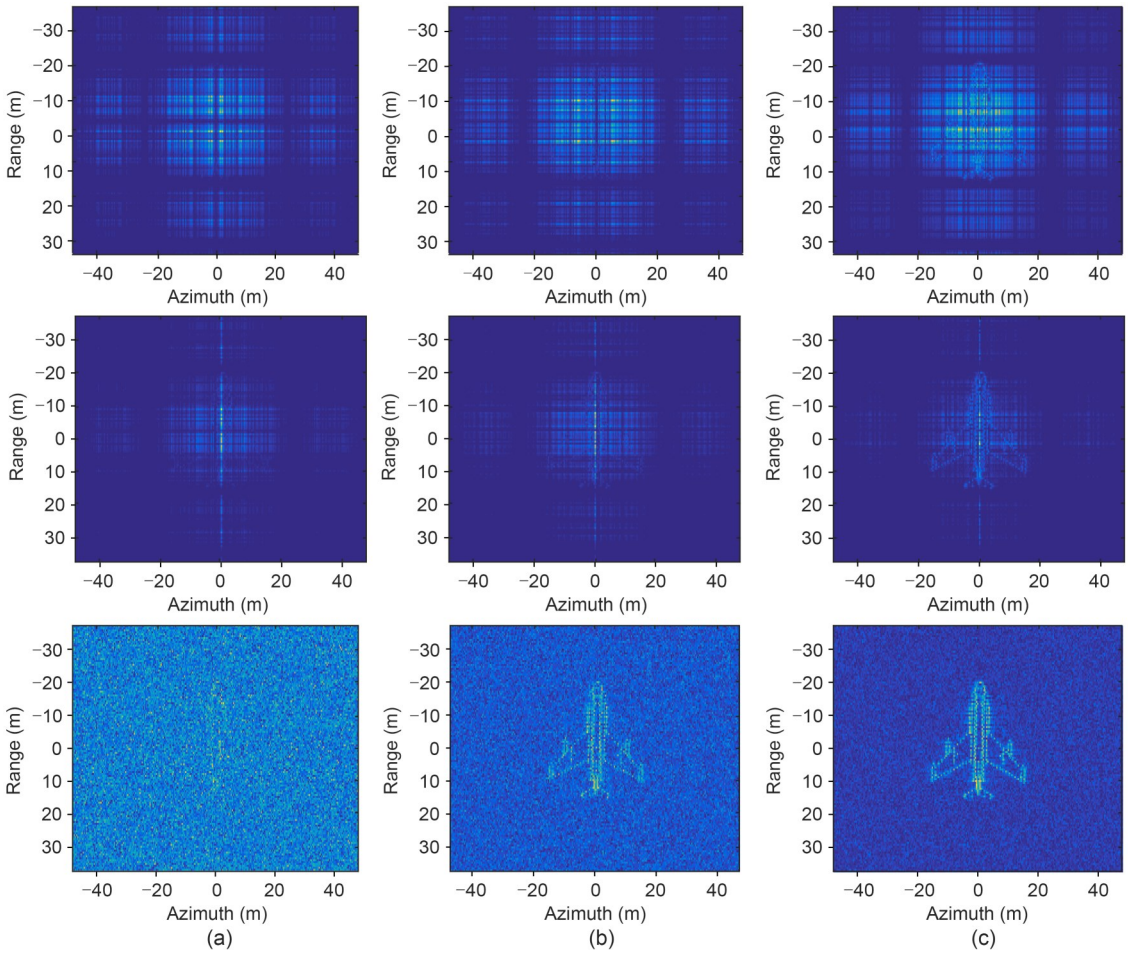

Fig. 10 Jamming performances with different jamming powers, where the first row is with the proposed method, the second row is with the ISRJ-based method, and the last row is with the conventional noise jamming method: (a) P_j=100 W; (b) P_j=50 W; (c) P_j=5 W

As shown in Fig. 8, the location range of the plane in the scene is [−15 m, 15 m] in the azimuth direction and [−15 m, 20 m] in the range direction. Then, the average suppression ratio is calculated in this scope. The results are presented in Fig. 11, where the duty ratios are set as η=η_A=0.5.

As shown in Fig. 11, obviously, the proposed nonperiodic phase modulation jamming method can obtain a larger average suppression ratio than both the ISRJ-based method and conventional noise jamming method. In this simulation scene, the average suppression ratio of the proposed method is approximately 20 dB larger than that of the ISRJ-based method with the same parameter settings and is approximately 27 dB and 30 dB larger than that of the noise jamming when the code widths are set as τ=10 μs, τ_A=2 ms and τ=20 μs, τ_A=4 ms, respectively. Hence, it can be concluded that the proposed method can obtain much better blanket shielding performance than the other two methods. In addition, the average

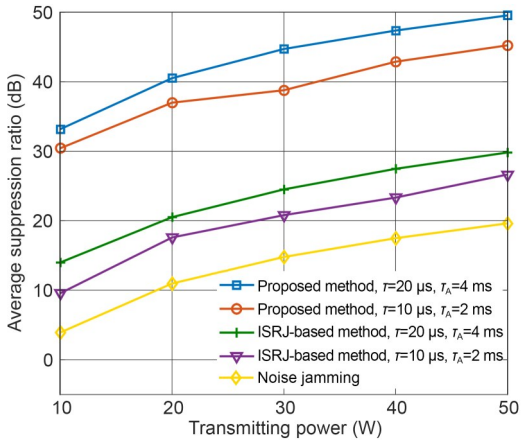

Fig. 11 Average suppression ratio

suppression ratio of the proposed method when τ=20 μs and τ_A=4 ms is approximately 3 dB larger than that when τ=10 μs and τ_A=2 ms. This demonstrates that a larger code width (i.e., a smaller coverage) is more beneficial to obtain a better jamming performance due to the energy concentration.

5 Measured data experiment

In this section, a measured unmanned aerial vehicle (UAV) data experiment is conducted. Considering that the jamming properties and the quantitative evaluations are presented in detail in Section 4, the main purpose of this UAV data experiment is to further verify the validity of our proposed method.

The Pioneer UAV model is given in Fig. 12a. The length of the UAV is approximately L_R=2.3 m and the wingspan is approximately L_A=2.9 m.

(a) (b)

Fig. 12 The measured Pioneer UAV data experiment: (a) target model; (b) imaging scene in the microwave chamber

The imaging data of the UAV are obtained in the microwave chamber, as shown in Fig. 12b. The parameters of the stepped frequency chirp signal are listed in Table 1.

With the listed parameters, the phase modulation parameters should satisfy $\tau \leq 32$ μs and $\tau_A \leq 8.3$ ms according to Eqs. (39) and (40), respectively. Assume that the jammer is fixed on the center of the UAV. According to the parameter constraints above, Fig. 13 presents the jamming results with different modulation parameters, where the jamming power is equivalently converted according to the imaging scenes, and the duty ratios are set as $\eta=\eta_A$=0.5.

Table 1 Signal parameters

Parameter	Value
Radio frequency (f_0)	8 GHz
Subpulse width (T_p)	1 μs
Subpulse bandwidth (B)	10 MHz
Subpulse repetition interval (T_r)	5 μs
Frequency interval (Δf)	20 MHz
Subpulse number (N)	201
Dwell time within one aperture (T_d)	2 ms
Observation aperture number (M)	116
Rotation angular velocity (ω)	0.55π rad/s

As shown in Fig. 13a, when jamming is not executed, the UAV is clearly visible in the center of the image, whose shape and size are consistent with those of the actual target model. After the proposed phase modulation jamming, the UAV is completely covered by the generated high-level blanket sidelobes and becomes unrecognizable, as shown in Figs. 13b and 13c. Hence, it can be concluded that the validity of the proposed method is verified by the measured UAV data experiment.

To present the high-level blanket sidelobes generated by nonperiodic phase modulation more visually, Fig. 14 further presents the range cuts of Fig. 13 when the azimuth coordinate is equal to 0.5 m, where the amplitudes are all normalized based on the original unjammed image. As shown in Fig. 14a, for

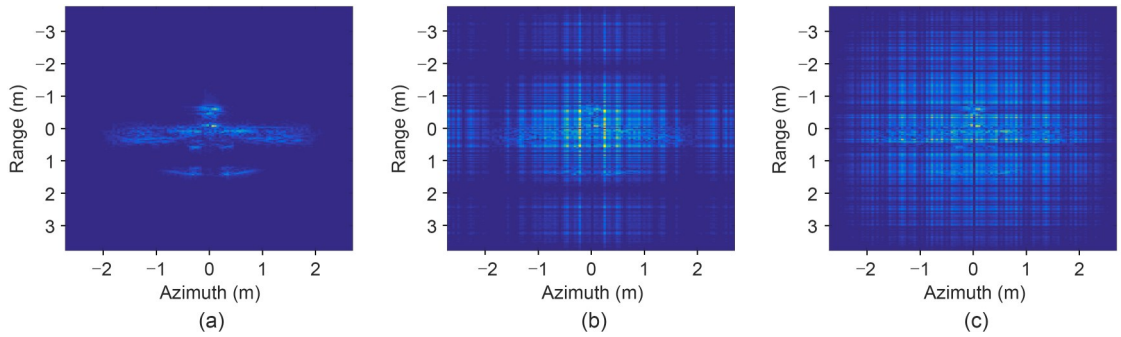

Fig. 13 Jamming performances with the measured UAV data experiment: (a) original unjammed image; (b) jammed image with τ=20 μs and τ_A=6 ms; (c) jammed image with τ=10 μs and τ_A=4 ms

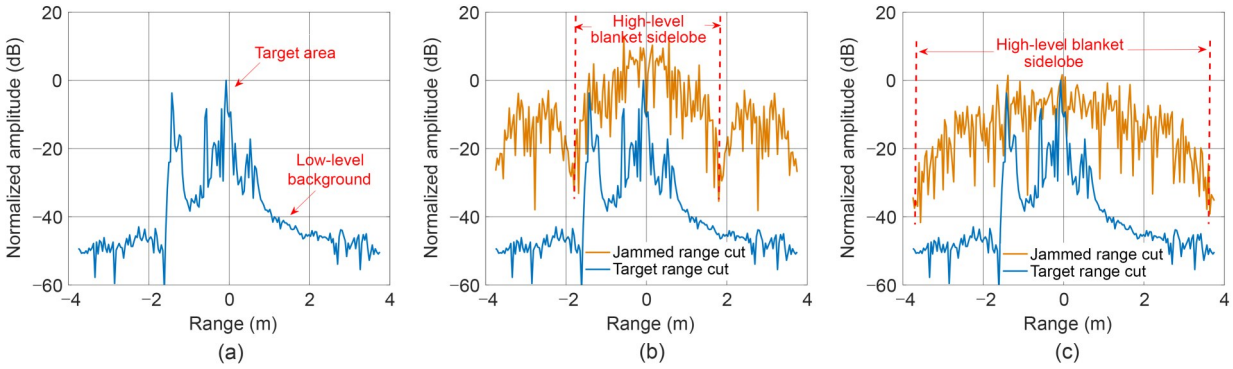

Fig. 14 Range cut at the azimuth 0.5 m: (a) original unjammed image; (b) jammed image with τ=20 μs and τ_A=6 ms; (c) jammed image with τ=10 μs and τ_A=4 ms. References to color refer to the online version of this figure

the original unjammed range cut, the amplitude of the target area is much larger than that of the low-level background (approximately 40 dB in the image). After jamming, high-level blanket sidelobes are generated instead of the low-level background, whose amplitude is also obviously much larger than those of the target area (approximately 30 dB in Fig. 14b and 20 dB in Fig. 14c). The generated sidelobes perfectly cover the target and make it unrecognizable. In addition, when the code widths are set as τ=20 μs and τ_A=6 ms, the coverage of the blanket area is approximately 3.75 m, as shown in Fig. 14b. When the code widths are set as τ=10 μs and τ_A=4 ms, the coverage of the blanket area increases to 7.5 m due to the reduction of the code width τ, while the amplitude of the sidelobes suffers approximately 10 dB loss comparatively, as shown in Fig. 14c. The results are consistent with theoretical analyses.

6 Conclusions

In this paper, a novel blanket jamming method against stepped frequency chirp radar is proposed using two-dimensional nonperiodic phase modulation. By intercepting and modulating the radar signal with a nonperiodic phase modulation pulse, the radar image will be covered by high-level blanket sidelobes spreading along both the range and azimuth directions. Both the Yake-42 plane data simulation and measured unmanned aerial vehicle data experiment results demonstrate the validity of the proposed method. In the future, the code design and optimization of the phase modulation to further improve the blanket performance will be our working directions.

Contributors

Qihua WU and Feng ZHAO designed the research. Qihua WU, Tiehua ZHAO, and Junjie WANG processed the data. Qihua WU and Feng ZHAO drafted the paper. Xiaobin LIU and Shunping XIAO helped organize the paper. Qihua WU and Feng ZHAO revised and finalized the paper.

Compliance with ethics guidelines

Qihua WU, Feng ZHAO, Tiehua ZHAO, Xiaobin LIU, Junjie WANG, and Shunping XIAO declare that they have no conflict of interest.

Data availability

The data that support the findings of this study are available from the corresponding authors upon reasonable request.

References

Bo Z, Zhou F, Shi XR, et al., 2015. Multiple targets deception jamming against ISAR using electromagnetic properties. *IEEE Sens J*, 15(4):2031-2038. https://doi.org/10.1109/JSEN.2014.2368985

Feng DJ, Tao HM, Yang Y, et al., 2011. Jamming de-chirping radar using interrupted-sampling repeater. *Sci China Inform Sci*, 54(10):2138-2146. https://doi.org/10.1007/s11432-011-4431-4

Feng DJ, Xu LT, Pan XY, et al., 2017. Jamming wideband radar using interrupted-sampling repeater. *IEEE Trans Aerosp Electron Syst*, 53(3):1341-1354. https://doi.org/10.1109/TAES.2017.2670958

Huang CJ, Chan EHW, 2021. Photonic-assisted microwave frequency and phase shifter for deception jamming. *IEEE Photon J*, 13(3):1-10. https://doi.org/10.1109/JPHOT.2021.3074164

Kang BS, Lee K, Kim KT, 2021. Image registration for 3-D interferometric-ISAR imaging through joint-channel phase difference functions. *IEEE Trans Aerosp Electron Syst*, 57(1):22-38. https://doi.org/10.1109/TAES.2020.3021108

Luo Y, Zhang Q, Qiu CW, et al., 2010. Micro-Doppler effect analysis and feature extraction in ISAR imaging with stepped-frequency chirp signals. *IEEE Trans Geosci Remote*

Sens, 48(4):2087-2098. https://doi.org/10.1109/TGRS.2009.2034367

Meller M, 2012. Cheap cancellation of strong echoes for digital passive and noise radars. *IEEE Trans Signal Process*, 60(5):2654-2659. https://doi.org/10.1109/TSP.2012.2187286

Moradikia M, Samadi S, Cetin M, 2019. Joint SAR imaging and multi-feature decomposition from 2-D under-sampled data via low-rankness plus sparsity priors. *IEEE Trans Comput Imag*, 5(1):1-16. https://doi.org/10.1109/TCI.2018.2881530

Pan XY, Wang W, Feng DJ, et al., 2014. On deception jamming for countering bistatic ISAR based on sub-Nyquist sampling. *IET Radar Sonar Nav*, 8(3):173-179. https://doi.org/10.1049/iet-rsn.2013.0020

Rong JJ, Wang Y, Han T, 2019. Iterative optimization-based ISAR imaging with sparse aperture and its application in interferometric ISAR imaging. *IEEE Sens J*, 19(19):8681-8693. https://doi.org/10.1109/JSEN.2019.2923447

Tai N, Cui KB, Wang C, et al., 2016. The design of a novel coherent noise jammer against LFM radar. *IEICE Electr Expr*, 13(21):2138-2149. https://doi.org/10.1587/elex.13.20160924

Wang C, Zhang QY, Hu JM, et al., 2022. An efficient algorithm based on CSA for THz stepped-frequency SAR imaging. *IEEE Geosci Remote Sens Lett*, 19:4006505. https://doi.org/10.1109/LGRS.2020.3039958

Wang JJ, Feng DJ, Xu ZM, et al., 2021. Time-domain digital-coding active frequency selective surface absorber/reflector and its imaging characteristics. *IEEE Trans Antenn Propag*, 69(6):3322-3331. https://doi.org/10.1109/TAP.2020.3037757

Wang JJ, Feng DJ, Kong YM, et al., 2022. Imaging properties of nonperiodic time-varying active frequency selective surface. *IEEE Trans Antenn Propag*, 70(7):5884-5891. https://doi.org/10.1109/TAP.2022.3161385

Wang W, Pan XY, Liu YC, et al., 2014. Sub-Nyquist sampling jamming against ISAR with compressive sensing. *IEEE Sens J*, 14(9):3131-3136. https://doi.org/10.1109/JSEN.2014.2323978

Wang XS, Liu JC, Zhang WM, et al., 2007. Mathematic principles of interrupted-sampling repeater jamming (ISRJ). *Sci China Ser F Inform Sci*, 50(1):113-123. https://doi.org/10.1007/s11432-007-2017-y

Wang Y, Bai XR, Zhou F, 2022. High-resolution inverse synthetic aperture radar imaging with sparse stepped-frequency chirp signals under low signal to noise ratio. *J Electr Inform Technol*, 44(3):1034-1043 (in Chinese). https://doi.org/10.11999/JEIT210056

Wu QH, Liu J, Wang JJ, et al., 2018. Improved active echo cancellation against synthetic aperture radar based on nonperiodic interrupted sampling modulation. *IEEE Sens J*, 18(11):4453-4461. https://doi.org/10.1109/JSEN.2018.2824351

Wu QH, Zhao F, Ai XF, et al., 2019. Two-dimensional blanket jamming against ISAR using nonperiodic ISRJ. *IEEE Sens J*, 19(11):4031-4038. https://doi.org/10.1109/JSEN.2019.2897363

Xu G, Xing MD, Xia XG, et al., 2015. High-resolution inverse synthetic aperture radar imaging and scaling with sparse aperture. *IEEE J Sel Top Appl Earth Obs Remote Sens*, 8(8):4010-4027. https://doi.org/10.1109/JSTARS.2015.2439266

Xu LT, Feng DJ, Liu YC, et al., 2015. A three-stage active cancellation method against synthetic aperture radar. *IEEE Sens J*, 15(11):6173-6178. https://doi.org/10.1109/JSEN.2015.2453396

Zhang L, Qiao ZJ, Xing MD, et al., 2011. High-resolution ISAR imaging with sparse stepped-frequency waveforms. *IEEE Trans Geosci Remote Sens*, 49(11):4630-4651. https://doi.org/10.1109/TGRS.2011.2151865

Zhang Q, Zeng YS, He YQ, et al., 2008. Avian detection and identification with high-resolution radar. IEEE Radar Conf, p.1-6. https://doi.org/10.1109/radar.2008.4721116

Zhao ZK, Zhou WB, Li H, 2021. LFM radar jamming technology based on non-integer order SSC blind frequency shift. *J Electr Inform Technol*, 43(10):2824-2831 (in Chinese). https://doi.org/10.11999/JEIT200748

Zhou F, Tian XD, Wang Y, et al., 2021. High-resolution ISAR imaging under low SNR with sparse stepped-frequency chirp signals. *IEEE Trans Geosci Remote Sens*, 59(10):8338-8348. https://doi.org/10.1109/TGRS.2020.3045971